Article:

Yang, S, Wang, Z, Wang, J et al. (5 more authors) (2022) Defect segmentation: Mapping tunnel lining internal defects with ground penetrating radar data using a convolutional neural network. Construction and Building Materials, 319. 125658. ISSN 0950-0618

https://doi.org/10.1016/j.conbuildmat.2021.125658

Defect segmentation: Mapping tunnel lining internal defects with ground penetrating radar data using a convolutional neural network

Senlin Yang[b,c], Zhengfang Wang[a], Jing Wang[a,*], Anthony G. Cohn[d,e], Jiaqi Zhang[a], Peng Jiang[c], Lichao Nie[b,e], Qingmei Sui[a]

[a]*School of Control Science and Engineering, Shandong University, Jinan, 250061, China.*
[b]*Geotechnical and Structural Engineering Research Center, Shandong University, Jinan, 250061, China*
[c]*School of Qilu Transportation, Shandong University, Jinan, 250061, China*
[d]*School of Civil Engineering, Shandong University, Jinan, 250061, China*
[e]*School of Computing, University of Leeds, Leeds, LS29JT, UK*

Abstract

This work offers a defect segmentation approach for the nondestructive testing of tunnel lining internal defects using Ground Penetrating Radar (GPR) data. Given GPR synthetic data, it maps the internal defect structure, using a CNN named Segnet coupled with the Lovász softmax loss function, which enhances the accuracy, automation, and efficiency of defect identification. Experiments with both synthetic and actual data show that our innovative method overcomes problems in standard GPR data interpretation. A physical test model with a known defect was developed and manufactured, and GPR data was acquired and analyzed to verify the approach.

Keywords: Convolutional Neural Networks (CNNs), Ground Penetrating Radar (GPR), GPR Data Intelligent Recognition, Tunnel Lining Defect

1. Introduction

Tunnels are vital components of traffic and water-conservation projects, and their safe operation has always been a concern for engineers[1]. A variety of defects in tunnel lining commonly appear over the service life due to age, geological circumstances, and natural weathering, which can lead to tunnel instability and jeopardize tunnel operation safety. Defects in tunnel lining can be categorized

*Corresponding author

Email addresses: `yangsenlin@mail.sdu.edu.cn` (Senlin Yang), `wangzhengfangsdu@hotmail.com` (Zhengfang Wang), `wangjingkz@sdu.edu.cn` (Jing Wang), `A.G.Cohn@leeds.ac.uk` (Anthony G. Cohn), `201934530@mail.sdu.edu.cn` (Jiaqi Zhang), `sdujump@gmail.com` (Peng Jiang), `llichaonie@163.com` (Lichao Nie), `qmsui@sdu.edu.cn` (Qingmei Sui)

into two types: external defects, such as external cracks and leakages, which can be directly observed and internal defects, observable by other means. Common types of tunnel lining internal defects include cracks, voids, lining-rock separation, water seepage, and other structural defects, which affect the stress and erosion on the tunnel differently[2–4]. It is critical to accurately classify, locate, and shape any lining internal defects in order to maintain the tunnel's safety.

Common detection methods for tunnel lining internal defects include direct methods for extracting centroid detection and nondestructive testing (NDT) techniques such as infrared thermography, multispectral analysis, ultrasonic pulses, and Ground Penetrating Radar (GPR), et al[5–7]. Because of its fast detection speeds, excellent penetrating ability, convenience, and portability[8], GPR is preferred for defect detection in tunnel linings. Research on tunnel integrity detection using GPR dates back to 1994 [9], and numerousrous researchers have investigated the performance of GPR [10–12], which has evolved into a discipline.

By producing electromagnetic waves and receiving reflected signals, GPR may identify tunnel lining interior structures based on variances in relative dielectric constants. These reflected signals are hyperbolic and frequently interlaced, making data interpretation challenging. To derive the relative dielectric constant model, theoretical migration imaging and inversion are frequently utilized[13, 14]. Furthermore, much research has been conducted on the automated detection of abnormal objects in GPR data using pattern recognition and machine learning. Pasolli et al.[15] used a genetic algorithm and a support vector machine (SVM) to perform pattern recognition and classification on pre-processed GPR data and achieved relatively accurate identification. Xie et al.[16] used SVM to extract the void signal from synthetic GPR data and collected real data through model tests to apply to the method. Although 97.74% accuracy was obtained, it is difficult to use their method to accurately obtain the position and shape of the voids. Dou et al.[17] and Zhou et al.[18], respectively, proposed a C3 clustering algorithm and an optimized stable clustering algorithm (OSCA) to extract complex GPR reflection signal characteristics and afterward fitted them to GPR reflection hyperbola parameters.

Deep learning methods based on convolutional neural networks (CNNs) have brought new solutions for GPR data processing and defect recognition as artificial intelligence has advanced rapidly in recent years. Methods such as the fully convolutional network (FCN)[19], U-net[20], and Segnet[21] have continuously developed in the realm of image and computer vision, and are now being applied to autopilot systems and other applications. CNNs have also been used in the medical field to discover and identify defects[20, 22, 23]. In geophysics, several investigations have been conducted using CNNs and related methods to solve the inversion problem[24–26]. Li and Liu et al. developed SeisInvNet based on fully connected and convolutional network to successfully reconstruct spatial velocity model from timeseries data and get a more accurate result than that by traditional DNNs[24]. Based on this, Liu et al. further improved SeisInvNet by optimizing Encoder mode, increasing applicability of SeisInvNet on the realistic structural model[27]. This is the bright spot and excellent progress of seismic intelligent inversion technology

CNNs have been widely employed in the detection of external faults in buildings to analyze huge quantities of structural surface pictures and to identify and classify the defects. Young-Jin Cha et al. conducted in-depth research on this aspect and successfully identified concrete cracks, steel corrosion, and other defects using a CNN network[28, 29]. They also created a semantic damage detection network (SDDNet)[30] that was especially intended for superficial cracks in buildings and produced excellent results while decreasing the number of network parameters and considerably boosting computational performance. Miao et al.[31] used the improved U-net with a Se-ResNet block to train tunnel defects images for a highway tunnel and alleviated the imbalance problem of crack results; tunnel sidewall defects were accurately identified. For GPR data recognition, Nuaimy et al.[32] effectively combined GPR data processing, pattern recognition, and neural networks to complete high-resolution labeling, imaging, and classification of GPR data as early as 2000, which provided a reference for the application of neural networks in solving the GPR data interpretation problem. Xu et al.[33] used vehicle-borne GPR to detect railway subgrade defects and applied the Faster R-CNN method to identify defect signals in GPR data. Their research effectively obtained the position, classification, and probability of defects in GPR data image. In terms of GPR detection on asphalt pavements, Tong et al.[34] designed a recognition CNN, location CNN, and feature extraction CNN, for the automatic recognition, location, length measurement, and 3D reconstruction of cracks, respectively.

The research methods reviewed above mainly identified defect signals in GPR data images, allowing for accurate classification and positioning. However, it is necessary to improve the accuracy, automation, and efficiency of GPR data interpretation for tunnel linings internal defects, and to obtain the classification and internal structures of linings.

We have explored the potential of mapping the tunnel lining internal structure, including the classification, position, and form of the defects, using GPR data, inspired by the advancement of semantic segmentation in computer vision[19–21]. As a result, this article presents a novel approach for completing GPR data processing and obtaining information on tunnel lining internal defects, which we term defect segmentation. A two-dimensional sideline is employed in actual detection, and we reduce the issue into two-dimensional data and model. In this method, precise information on the tunnel lining internal material structure may be acquired, which is more automated and understandable, after GPR data is routinely processed and utilized as input. The efficiency and usefulness of tunnel fault detection may be substantially improved with our method. We focus on effective synthetic data preparation, CNN selection and analysis, as well as real-world data application. The remainder of the paper is laid out as follows: In Section 2, we describe the characteristics of our proposed method and provide designed dielectric constant models and corresponding synthetic GPR data for the training of CNNs. We then design CNNs based on the characteristics of GPR data and introduced the detailed parameters of the CNNs in Section 3. The performance of the proposed CNN is discussed, comparing different CNNs and different defects. Section 4 reports on the results obtained from analyzing synthetic data, whereas Section 5 focuses on evaluating the performance of the method using real data derived from a test model. Finally, in the conclusion, we summarize the paper's contributions.

2. Method description and GPR data preparation

2.1. Method description

The working principle of GPR is as follows: the electromagnetic wave excited by the GPR encounters the dielectric difference present in the detected area and the signal is reflected and acquired, allowing the structure and anomalies of the detected area to be inferred. In complicated internal structures, the acquired data is stacked with similar shapes, making it very difficult to properly separate them and derive meaning.

The defect segmentation we propose addresses problems that exist in such complex detected areas that may include rebars, surrounding rocks, and multiple defects. The relative dielectric constant model within a tunnel lining is denoted M, and the resultant GPR data is denoted D. M may be segmented to produce a classification, C, of the image data reflecting the model's components. Thus we may characterize the task as follows:

$$D = f(M), \tag{1}$$

$$C = seg(D), \tag{2}$$

where seg is the mapping from GPR data D to defect segmentation M, and f represents the process of collecting GPR data for the internal model of the lining, which is shown in Fig. 1.

For classification problems, because the dielectric constant of the same material is within a specific range, it is a many-to-one problem; that is, for the same C, D is not fixed, which is different from the inversion problem[26].

2.2. CNN theory

CNNs have become one of the most significant application methods of deep learning due to their wide use in image processing. They can extract features from the input data and then perform tasks such as classification, recognition or prediction. Especially for semantic segmentation, CNNs achieved superior results to traditional methods due to their pixel feature extraction, weight sharing and powerful nonlinear mapping capabilities[35]. CNN parameters θ, such as convolution kernel and bias, can be obtained by the features and relationships extracted from a huge number of model-data pairs, and nonlinear functions f are constructed. Then the mapping of input D_{in} to output D_{out} will be achieved, as shown

$$D_{out} = f(\theta, D_{in}). \tag{3}$$

Table 1: Relative dielectric constant and conductivity properties of different media

Media	Relative dielectric constant	Conductivity S/m
Air	1	0
Water	81	0.0005
Rebar	300	10ˆ8
Surrounding rock	6∼8	0.001
Concrete	8∼10	0.0001

In this process, D_{in} is the input to the CNN, allowing prediction result $\bar{D}_{out}$ to be obtained. The difference between the predicted $\bar{D}_{out}$ and the real target D_{out} is calculated by the chosen loss function to get the gradient, which would be used to update the CNNs parameters θ. Based on a large number of D_{in} -D_{out} pairs and multiple iterations, network parameters can finally be obtained. Susequently, only the real data D is required as an input to the trained CNNs, and the correct defect category, location, and shape can be quickly obtained. This makes the interpretation of GPR data simple, automatic and efficient. The workflow is shown in Fig.2.

2.3. Tunnel lining interior materials and defects

As previously stated, the CNN's training method is based on a huge number of model-data pairings. It is difficult to collect structural information inside the tunnel lining to serve as a labeled model correlating to our GPR data, unlike the identification of apparent disease. This issue can also be seen in geophysical inversion. Li and Liu et al.[24–26] have successfully introduced transfer learning in deep learning based inversion of seismic data, electrical resistivity data and GPR data, and realized the effective application of deep learning network in field testing on the network trained with synthetic data, which is a great impetus to the application of deep learning in geophysics. Therefore, we also use synthetic data to provide a large number of model-data pairs and propose a transfer learning on real-world data to address the problem. The prediction result of CNNs depends on the model used to train it, making the practical analysis and selection of tunnel lining materials as well as the correct design of the tunnel lining models a focus of our study.

Rebars, rock, voids, fractures, linear-rock separation, and water seepage are all common tunnel lining interior materials and defect kinds. They are divided into five categories: air, water, concrete, surrounding rock, and rebar. Table 1 shows their respective dielectric constants and conductivity ranges, which have been adjusted based on [36]. Water and air are two faulty media that may be found in voids, cracks, and lining-rock separations. Rebars and rocks may be present within the tunnel lining, which influences and confuses GPR data. Due to differences in dielectric constants and electrical conductivity, various materials have varied impacts on GPR, which is the basis for our defect detection.

The materials and defects in the designed model can be divided into nine types: rebar, concrete, rock, crack, water-bearing crack, void, water-bearing void, lining-rock separation, and water-bearing separation. The lining-rock separation is a defect that appears between the lining and the surrounding rock, and a void is inside the concrete. Separations and voids cause different hazards; thus despite their similar shapes, different types are used here[4, 37]. Cracks are small defects that arise from uneven forces in the tunnel. They are also present in the concrete and severely affect the tunnel lining bearing capacity[38]. These three types (i.e. separations, voids, and cracks) are further expanded into six types of defects according to whether they contain water or not. Combined with three types of tunnel lining materials (i.e. rebar, concrete, and rock), a total of nine types are obtained, which will be the target types for our defect segmentation.

Through the arrangement and combination of the above nine types materials and defects, we can get the models for training. In order to focus on the influence of the existence of rebars and whether the defect contains water on the segmentation results, they are divided into the following categories:

(1) No defect in tunnel lining;
(2) A water-free defect in tunnel lining without rebar;
(3) A water-bearing defect in tunnel lining without rebar;
(4) A water-free defect in tunnel lining with rebar;
(5) A water-bearing defect in tunnel lining with rebar.

For the purpose of generating training data, we split these categories further. (1) is split into four combinations depending on whether it contains rock, rebar, both or neither. Each of the categories (2-5) are split into 12 possible combinations. These result from whether there are one or two defects and whether the defects contain water or not. We use 2D models and data since the network requires a lot of training data and this simplifies the network's parameters. Based on the above categories, we created 52 model combinations and 2,400 models for each combination, totaling 124,800 sets of tunnel lining relative dielectric constant models for deep learning algorithms, covering the majority of scenarios. In the designed model, symmetrical quasi circles are used as rebars; thin lines with a width of 1-3 grid cells are used as cracks; considering the randomness of the voids, randomly generated irregular shapes are used to fit cavities in different states. The randomly generated interface separates the concrete from the rock, and the lower part is rock. The lining-rock separation is a random shape attached to the interface. Finally, referring to Table 1, the relative dielectric constant is set, and realistic models can be obtained. The grid size of the model is 70×200, and the length and width of each cell is $0.01m$, that is, the model has an actual width of $2.0m$ and depth of $0.7m$.

Due to the difference in electromagnetic characteristics of different materials (such as air and water), the propagation of the electromagnetic waves is affected, and reflected waves are generated. This reflected signal is then received by the GPR antenna. For CNN training, the closer the simulated data is to the real GPR data, the stronger the applicability of the network. To generate data in batch mode, referring to previous work[26], the finite difference time domain (FDTD) method based on in-house MATLAB code used, combined with a 10-layer convolutional perfect matching layer[39], for modeling of GPR data. Combined with the electrical parameters mentioned in Table 1, the FDTD and CPML are robust, as demonstrated in previous work, and can be effective in subsequent real-data applications. For models of size 70×200, a Ricker wavelet with a main frequency of 600 MHz is used, and each model uses 99 sidelines. The sampling time interval is 2.3587×10^{-11}, with a total sampling of 800 steps. So the size of the input GPR data is 800×99. As noted above there 124,800 synthetic training data instances, which are given as input to the network.

3. Convolutional Neural Networks for defect segmentation

Many classical CNNs, such as Segnet[21], U-net[20], have achieved impressive results not only for semantic segmentation, but also in other tasks, such as medical recognition, geophysical data recognition, et al. In recent years, the DeepLab series[40–42], proposed between 2017 and 2018, has now become one of the most popular novel networks used for semantic segmentation. In view of the wide range of applications and applicability, these CNNs were chosen to compare their effectiveness on defect segmentation, with a novel loss function introduced. Network hyperparameters were set to update the parameters reasonably and effectively in the training process.

The method of defect segmentation is similar to the semantic segmentation often performed in CNNs but more complicated. It has the following features:

(1) First, GPR data and dielectric constant models differ in shape, value, and distribution. Our goal model is a spatial structure with a size of $h \times w$, where h and w represent the depth and width of the model respectively, and GPR data is a time series measured at different positions in the horizontal direction with a size of $nt \times w$, where nt represents the time step. There are differences in image processing of detection data between time series and space series. The hyperbolic shapes dominate the response to various internal structures in GPR signal, and their morphology is more similar and indistinguishable than ones in natural images. The shapes of voids and the separations are similar, but their locations are different. The location of the defects need to be considered, and their differences and features are extracted from similar and complex data. In addition, for defects and materials of the same shape, the location and polarity of the reflected signal is affected by different dielectric constants and whether they contain water. As shown in Fig. 3 (a) and (b), the dielectric constants of concrete in the two models are different, which leads to differences in their GPR data, as shown in the yellow box; however, the fault segmentation results are the same. Comparing Fig. 3 (b) and (c) shows how the water content of the defect affects the signal polarity, considering the shape information and amplitude of the signal. That is, the model is influenced by both shape and value. The CNN needs to consider both numerical information and shape characteristics. Given that our present problem is a classification

task, we suggest that a properly selected CNN is more suitable for defect segmentation than GPRInvNet, which focuses on inversion.

(2) The size of normal data and data representing defects is unbalanced. As shown in Fig. 3(b), the size of the rebars and cracks are small, yet they have a great impact on the GPR data. This size imbalance creates a particular problem for the prediction task, that is, defect segmentation. An effective loss function must be constructed and used in order to produce fine-grained resolution prediction results.

(3) To include all possibilities and avoid overfitting, a large amount of data and measurements are required for training, and the computational efficiency of the network needs to be taken into account.

We compared Segnet, U-net and DeepLab V3+ based on the aforementioned analysis. We found that Segnet has the advantages of a simple network structure, fewer parameters, and superior quality results. In addition, Segnet uses max location in upsampling to provide useful information during decoding, which improves the provision of structural information and improved high-frequency data correspondence.

3.1. Segnet

Segnet uses high-dimensional compression data, through convolution and pooling, to obtain high-dimensional features of an image and afterwards upsampling to complete the regression and segmentation of the image. In the network, the size of the convolution kernel is 3×3. To prevent gradient anomalies, batch normalization(BN) is employed and a rectified linear unit ($ReLU$) is used as the activation function in other layers, with the exception of the last layer. As a semantic segmentation problem, softmax is utilized as the activation function of the last layer to obtain the probability under each classification to complete the segmentation. The innovation of Segnet is that the low-resolution feature maps are converted to a high-resolution feature map using the upsampling method during the decoder process, which differs from FCN and U-net deconvolution. Specifically, features are compressed by pooling in the encoder section, and the index of each pooling is saved, that is, the original maximum position is saved. Then the corresponding pooling index is used in the decoder for nonlinear upsampling. In this way, sparse upsampling feature maps can be obtained without learning the weights used in the deconvolution. Badrinarayanan et al.[21] compared Segnet with common CNNs and proved that Segnet is superior to other methods for region classification. Because Segnet is used for image semantic segmentation with fewer parameters and better results, our main objective was to study the defect segmentation of GPR data by Segnet. Its specific structure is as shown in Fig. 4. Segnet has few parameters, maintains high-frequency information integrity, and achieves improved results compared to competing methods. In Section 4.2, a comparison between Segnet, U-net and DeepLab V3+ proves that Segnet is more suitable for the problem of defect segmentation.

3.2. Loss function

The cross-entropy loss function is the most often utilized loss function in semantic segmentation. The activation function of the classification problem is softmax, and the use of the L2 norm loss would severely affect gradient calculations and network updates. Using the logarithm, the cross-entropy loss function can alleviate the problem of gradient disappearance. The cross-entropy loss function is

$$L_{CE} = -\frac{1}{p}\sum_{i=1}^{p} \log y_i^*, \tag{4}$$

where i is the corresponding position of each grid cell, and y_i^* is the predicted probability of the corresponding position and label.

However, although the effect of the cross-entropy loss function has been proven in semantic segmentation, the results of the prediction need to be improved. This improvement is especially necessary for smaller objects because CNNs using the cross-entropy loss function often have difficulty predicting them. This makes it difficult to meet the requirement of detecting rebars and cracks using our method. Although rebars and cracks are noticeably reflected in the input data, rebars and cracks are usually very small and require high-resolution processing to be effectively classified in the segmentation. To solve this problem, we applied the Lovász softmax loss function in our CNN. The Lovász softmax loss function, as shown in Equation (5), was proposed by Berman in 2018 [43] to optimize mean intersection over union (MIoU), and its superiority on small objects is proven.

$$L_{LZS} = \frac{1}{|N|}\sum_{c=1}^{N} \overline{\Delta Jc}(m(c)), \tag{5}$$

where $\overline{\Delta Jc}$ is the Lovász extension to ΔJc,the approximation to the Jaccard index of class c, N is the number of material and defect classes–nine in this paper, and $m(c)$ is a vector of grid cell errors for class c.

Eerapu et al.[44] combined the cross-entropy and the Lovász softmax loss function to achieve better a MIoU. In this study, we also use the composite loss function:

$$L_{sum} = L_{CE} + L_{LZS}. \tag{6}$$

The results in Section 4.2 show that the addition of the Lovász softmax loss improved the quality of the results, especially for cracks.

3.3. Network hyperparameters

Suitable network hyperparameters improved the training results of the network. We used PyTorch to implement both the CNN and the Adam optimizer in this study. The batch size of the Adam optimizer was set to 24, and the initial learning rate was 5×10^{-5}. The network was trained for a total of 100 epochs to obtain sufficient parameter updates.

Considering the similarity of GPR data for different materials and defects, it is easy to overfit the network which severely affects the generalization ability of the network and even causes unreasonable network parameters. Therefore, avoiding the overfitting problem is an important task. For this, we applied both dropout and weight decay. Dropout was proposed by Hinton[45] in 2012 and is proven to effectively reduce overfitting to a specific feature by randomly discarding a few percentage points of the features. The weight decay[46] is used to add a L_2 regularization after the loss function, thereby reducing the complexity of the network coefficients, and improving the effectiveness of data fitting. In this paper, by comparison, the dropout probability was set to 20 % and the weight decay coefficient was 1×10^{-4}, which can effectively alleviate overfitting of the CNN.

4. Results and discussion

To effectively train the network, we divided 128,400 sets of model-data pairs in Section 2.3 into the training, validation, and test set with a ratio of 10:1:1, which were used to train CNNs, verify the ability of the CNNs to determine the optimal network parameters, and test the impact of the final network, respectively. Considering the different sizes of input GPR data and output model, we used bicubic interpolation to reshape the input data of 800×99 into 256×128. The size of the output is 128×256 and is cropped to 90×220 to reduce the impact of the CNN on the boundary. We trained four CNN-based networks: Segnet using the cross-entry loss function, Segnet using the cross-entropy and the Lovász maxsoft loss functions, and U-net and DeepLab V3+ using the cross-entropy and the Lovász maxsoft loss functions to compare their effects in the defect segmentation task. For reference, they are named Segnet (1 loss), Segnet(2 loss), U-net, and DeepLab V3+, respectively. An Intel Xeon (R) gold 6148 CPU with GTX Titan RTX GPU workstation was used for training the four networks. Because there are more than one hundred thousand groups of data, the training process takes more than 20 h, but after the training of the network, the defects segmentation of a group of data can be calculated in 0.01 s on average.

The loss function curve in the training and validation set is shown in Fig. 5. The result of Segnet(2 loss) is far superior to the comparative methods. As shown in Fig. 5(d), U-net and DeepLab V3+ have an overfitting on the validation set, whereas Segnet(2 loss) does not. To quantitatively evaluate the performance of the results of different CNNs and the results of dissimilar materials, a series of indicators were used, such as MPA, MIoU, Precision, and Recall.

4.1. Metrics

For a large amount of test data, it is inconvenient to show each result. Effective evaluation parameters should be used for the statistics of all results, so that the results of different methods and the impact of dissimilar materials can be analyzed.

Since they are already extensively used in semantic segmentation, mean pixel accuracy (MPA), MIoU, and frequency weighted intersection over union

(FWIoU) were chosen to evaluate the similarity of each prediction result and ground truth in this study for the comparison of different CNNs and different models. In MPA, the proportion of correctly classified pixels in each classification is separately calculated, and the mean of all categories is used to verify the correctness of the classification. MIoU is the most widely used classification and semantic segmentation standard. It represents the average of the ratio of the intersection and concatenation of each category's true and predicted values. FWIoU is an improvement on MIoU, which assigns weights to each class depending on how frequently they appear. Their equations can be found in [47]. In addtional, the predicted effect of each defects categories is evaluated using precision, recall, and F-measure. Precision refers to the percentage of properly predicted pixels in all prediction, and it may be thought of as a preference for correct predictions rather than complete prediction. The ratio of properly predicted pixels to all pixels in the actual category is known as recall, and it can be viewed as preferring complete prediction to correct predictions. In other words, the former is more applicable to analyzing the prediction effect of background, concrete, and rebars, which do not affect the category of defects discrimination; whereas the latter is more applicable to defects prediction because it must ensure the complete prediction of the target, even if there are redundant predictions. The F-measure, on the other hand, is a hybrid metric which is the harmonic mean of precision and recall[48].

4.2. Comparison of results with different loss functions, U-net and DeepLab V3+

The above comparison of the loss functions has shown the effectiveness of Segnet(2 loss) in tunnel lining defect segmentation. We also compare the performance of the three methods on the test set in Table 2, which also demonstrates the performance of Segnet(2 loss). Specifically, we selected four typical model-data pairs, as shown in Fig. 6. In conjunction with Table 3, the effects of each material and defect under each method were analyzed. In the Tables, optimal values are emboldened.

First, Segnet(1 loss) achieved acceptable results and had very accurate predictions for rebars, voids, and separations. However, it performed poorly for cracks and had the lowest precision. The recognition of cracks requires high resolution, which is more difficult for segmentation problems. As shown in Fig.6 (b) and (d), this method had a lower prediction accuracy for thinner defects such as cracks. The cross-entropy loss function focuses on the probability of each pixel but is limited to the overall effect, which results in a lower resolution of the result, making it difficult to identify small defects.

Second, Segnet(2 loss) performed optimally in all materials and defects. It accurately predicted the location and classification of cracks, voids, and separations, and was good for complex data. Good results are obtained for smaller defects, such as cracks and rebars. In general, most of the prediction results are accurate. The presence of reinforcing bars may cause some results to be incorrect, but the probability of errors is very low. This result proves the effectiveness of the Lovász Softmax loss and our method. In addtion, although

Table 2: Results of different methods

Metrics	Segnet(1 loss)	Segnet(2 loss)	U-net	DeepLab V3+
MPA	0.91	**0.93**	0.79	0.90
MIoU	0.83	**0.90**	0.75	0.84
FWIoU	**0.98**	**0.98**	0.96	**0.98**

Table 3: Results of different methods and different categories

Metrics	Methods	Lining Materials			Defects			Water-bearing Defects		
		Rebar	Concrete	Rock	Crack	Void	Separation	Crack	Void	Separation
Precision	Segnet(2 loss)	**0.9664**	**0.9968**	**0.9765**	**0.8157**	**0.9008**	**0.9111**	**0.8833**	0.8278	**0.8798**
	Segnet(1 loss)	0.9312	0.9961	0.9698	0.3108	0.8674	0.9019	0.8754	0.4164	0.8441
	U-net	0.9543	0.9875	0.9242	0.6324	0.8109	0.2918	0.2619	**0.9956**	0.7807
	DeepLab V3+	0.9163	0.9959	0.9732	0.5776	0.8386	0.9026	0.8680	0.6056	0.8163
Recall	Segnet(2 loss)	**0.9541**	**0.9969**	**0.9777**	**0.8039**	**0.8869**	0.8960	0.8740	**0.8303**	**0.8715**
	Segnet(1 loss)	0.9201	0.9928	0.9747	0.7889	0.8635	0.8923	0.8703	0.6922	0.8379
	U-net	0.9449	0.9861	0.9121	0.6495	0.8001	0.1930	0.1729	0.7064	0.7629
	DeepLab V3+	0.8751	0.9954	0.9757	0.6844	0.8422	**0.9076**	**0.8774**	0.7356	0.8156
F-measure	Segnet(2 loss)	**0.9602**	**0.9968**	**0.9771**	**0.8098**	**0.8938**	0.9035	**0.8786**	**0.8290**	**0.8756**
	Segnet(1 loss)	0.9256	0.9945	0.9723	0.4459	0.8654	0.8971	0.8728	0.5200	0.8410
	U-net	0.9495	0.9868	0.9181	0.6408	0.8054	0.2324	0.2083	0.6860	0.7717
	DeepLab V3+	0.8952	0.9956	0.9745	0.6265	0.8404	**0.9051**	0.8727	0.6643	0.8160

the importance of precision and recall for background and defect was discussed in Section 4.1, the precision and recall of the prediction results achieved using Segnet (2loss) are quite similar. When compared to the other methods, Segnet (2 loss) was the most stable approach with better metric values, which is critical for defect segmentation.

U-net performance was poorer than that of Segnet(1 loss). When multiple defects occurred at different depths in the same location, GPR data was more complicated. U-net made it difficult to effectively classify the defects, especially separations and cracks with water, as shown in Fig.6. The lack of accurate defect prediction seriously affects the judgment of the integrity of the tunnel lining. Through analysis, we believe that the network structure of U-net led to poor results. U-net saves the features of the encoded segments and uses them as feature maps when decoding, which is effective for the task of one-to-one correspondence in image semantic segmentation. However, for our task, GPR data and defect segmentation did not completely correspond, which caused U-net to introduce incorrect information and obtain poor results.

As a more advanced method in the field of semantic image segmentation, the overall effect of DeepLab V3+ is better than U-net, but slightly inferior to Segnet(2 loss). DeepLab V3+ further increases the eftectiveness of a decoder perhaps in the process of predicting the model on the basis of DeepLab V3, to recover the detailed object boundaries[49]. Although the spatial pyramid pooling module can further improve the receptive field and information in many aspects, like U-net, DeepLab V3+ does not apply well to the defect segmentation problem. For the given task, this decoder for boundaries is not suitable for the identification of defects with small size, which is why the performance on cracks and rebars in Table 3 is poor.

Table 4: Results of defect detection without rebars in different types of models

Class	Defects	Crack	Void	Separation	Crack&Void	Crack&Separation	Void&Separation
Water-free	MPA	0.96	0.98	0.97	0.91	0.95	0.95
	MIoU	0.93	0.96	0.95	0.86	0.91	0.92
	FWIoU	0.99	0.99	0.99	0.99	0.99	0.99
Water-bearing	MPA	0.96	0.97	0.97	0.90	0.93	0.94
	MIoU	0.93	0.96	0.95	0.84	0.88	0.91
	FWIoU	0.99	0.99	0.99	0.98	0.98	0.99

4.3. Results of different types of models

Through the above analysis, we demonstrated the effectiveness of Segnet and the Lovász softmax loss on defect segmentation and explained the unsuitability of U-net. Segnet also has different performance effects for different types of materials and defects. We divided the defect models into three categories and analyzed them in turn.

(1) Water-free defects in the tunnel lining without rebars
For defects in the tunnel lining without rebars, because the model is simple, our method produced accurate classification, location, and morphology in various defects, as shown in Fig. 7 and Table 4. Correct predictions are achieved on all models.

(2) Water-bearing defects in the tunnel lining without rebars
Similarly, the water-bearing defect was relatively simple, and the overall effect was satisfactory. It can be seen in Table 4 that crack detection performed less well than detection of other defects especially the model of cracks and voids, which shows that water-bearing defects had an impact on the results. As shown in Fig. 8 (c), especially when the void and crack are in the same horizontal position, the upper defect affects the data below, making it difficult to obtain an accurate shape, but the classification of the defects was accurate.

(3) Defect in the tunnel lining with rebars
The most challenging aspect of this method was that the rebars in the lining would seriously affect the internal defect signals acquisition. A row of rebars with a small diameter are reflected in GPR data as multiple parallel hyperbolae. They intersect each other, distorting the information below. In our results, the effect of rebars on the defect, especially cracks, was severe. As shown in Table 5, the models of "cracks and voids" under rebars, whether they contain water, have a MIoU value below 0.8, which was otherwise rare in our results. As shown in Fig. 9(c), the length of the crack was also incorrectly predicted, and the interface of the rock was also inaccurate in Fig. 9 (d). However, since correct classification and accurate positioning can meet most of our requirements, so the above problems have little effect in practice.

Our Segnet with two loss functions performed significantly better than Segnet with one loss function, U-net, and DeepLab V3+, both with two loss functions in terms of defect segmentation. Accurate classification and placement could be achieved in linings including cracks and rebars, demonstrating the

Table 5: Results of defect detection with rebars in different types of model

Class	Defects	Crack	Void	Separation	Crack&Void	Crack&Separation	Void&Separation
Water-free	MPA	0.91	0.95	0.96	0.84	0.89	0.91
	MIoU	0.86	0.91	0.94	0.78	0.84	0.87
	FWIoU	0.99	0.98	0.99	0.98	0.98	0.98
Water-bearing	MPA	0.91	0.94	0.96	0.83	0.89	0.90
	MIoU	0.86	0.90	0.94	0.76	0.83	0.85
	FWIoU	0.98	0.98	0.99	0.97	0.97	0.98

method's great precision. Despite significant difficulties with fault identification beneath rebars, most models were able to get the proper classification, which serves as a useful reference for post-processing. We believe that certain mistakes will inevitably occur due to the data's complexity.

5. Experiment on model testing

As a result of our network design and training, we obtained a CNN model which achieved excellent results on synthetic test data. Real data is more complicated than synthetic data, and noise and other disturbances seriously affect the quality of the collected data. In geophysics, because the detection area is usually unknown, many studies use physical model tests to verify the viability and applicability of theoretical methods[16, 50, 51]. To obtain GPR data from a known internal structure and verify the effect in a real environment, we built a test model to simulate the internal defects of a real tunnel lining. Real GPR data was collected, analyzed, and processed. At the same time, the CNN was fine-tuned to fit the real data. Finally, we used the CNN to segment the defects inside the tunnel lining with real data.

5.1. Model test building

We designed a test model using a rectangular concrete testbed with a size of $4.4m \times 2m \times 0.7m$ to simulate the internal structure of a tunnel lining, as shown in Fig. 10. Despite the fact that the GPR data were gathered on a rectangular testbed, the shape of the testbed had no major influence on the acquired data because a two-dimensional sideline was used. In the model, we used the materials employed in the lining of an actual tunnel. To simulate a water-bearing void, we used a PVC pipe with a length of 400 mm and a diameter of 120 mm to construct the separation. PVC pipes were filled with water, sealed at both ends and placed in the concrete to simulate a water-bearing void in the lining. As a result of this construction method, we knew the exact materials used and their shape within the model. On the model, we set two sidelines with a distance of $0.5m$ and a length of $4.4m$ to obtain reflection information of the embedded defects below the model, of which there was no defect below the X2 sideline. Through the X2 sideline, we could get enough background data under the current model for further experimental analysis and processing. The real GPR data was collected by Impulse Radar 600MHz equipment, with 512 sampling points. The mode of the GPR was set to 'Wheel', and the distance of the traces was chosen as $0.02m$. The GPR data was collected and transmitted to the computer via Wi-Fi.

5.2. Data processing

For the actual measured data, referring to previous research[26], we preprocessed the real GPR data, including time-zero correction, and removed the direct component, background signal, and bandpass filtering. In this way, clearer GPR data GPR data could be acquired, which improved the effectiveness of our method. To be more suitable for the real data, we used actual data from measurements of the plain concrete without defects, and randomly added it to the synthetic data as background noise. Because the size of the measured data and the synthesized data were different, we adjusted the measured data by the bicubic difference method and obtained hundreds of sets of background noise. These actual noise data sets were normalized, fixed to a reasonable range, and randomly added to the synthesized data. The updated synthetic data was used to train and fine-tune the CNN parameters for 40 epochs. In this way, the non-uniformity of the actual medium and the interference noise collected were considered, and the applicability of the CNN was further improved. This also provided a useful reference for real data processing under different operating conditions and environments in the CNNs method.

5.3. Result on real data

On the X1 sidelines, we tested the retrained CNN with real-world data. The internal structural information may be acquired instantly after the retrained CNN and data processing is completed, which increases the automation and efficiency of GPR data interpretation. Our method correctly predicted the categorization and location of water-bearing voids, as shown in Fig. 11, but the shape of the defect was poorly delineated. The data collected from the acquisition seems biased to the right (as shown in Fig. 11a) as a result of the real acquisition error and data processing, which impacts the recognition effect of our network. In the case of a single defect, our method achieves excellent results, demonstrating its viability. The potential of our method for real-world data was demonstrated through model building and effective data processing. It was useful to fine-tune the network based on the addition of real background and synthetic data, which may be necessary for the process of applying the CNNs method to real data.

6. Conclusion and future directions

In this paper, we used a CNN to build a new approach called defect segmentation to resolve the problem of GPR data interpretation and tunnel lining defects detection. The conclusions of this study are as follows:

- There are numerous differences between the defect segmentation of GPR data and semantic segmentation of natural images, including signal dissimilarity, morphological differences between the input and output, and the impact of the values on the results, making it difficult to directly apply CNNs to the task of GPR defect segmentation.

- The characteristics of Segnet make it a better fit for our method than U-net and DeepLab V3+, and we have demonstrated that it achieved more accurate results. Almost all models in a synthetic dataset were correctly classified, and an MPA of 93% and MIoU of 90% have been achieved with the cross-entropy and Lovász softmax loss functions.

- The Lovász softmax loss function is worth mentioning, especially for crack detection, because the approach substantially improves segmentation accuracy. A Segnet combining the cross-entropy and the Lovász softmax loss function improved 7% the MIoU as compared with a Segnet using cross-entropy.

- In the CNN method, the accuracy of the prediction findings was likewise strongly related to the complexity of the GPR data. Both water-bearing defects and rebars had an impact on the segmentation problem. The existence of rebars, as well as the GPR signal's reaction to them, had a significant impact on the signals of underlying defects, making prediction difficult.

- When applying our proposed CNN on actual data, we recommend collecting background signals from the related environment, combining existing synthetic data sets, and fine-tuning the network to improve outcomes.

Of course, there are still some deficiencies in this study, which will be taken as future research directions. It is worth noting that there are some deficiencies in the synthetic data generated by FDTD used in this study, such as not considering the dispersion of water, using 2D model and data, which will be the main research focuses in future. It is also important to improve our GPR data to be closer to real data, which is conducive to the promotion of the network in real data. The independent design of the network is also our key research in future. According to the characteristics of GPR data and cracks, adopting a more appropriate network structure will improve our results, such as SDDNet specially designed for cracks detection by Choi and Cha[30] and GPRInvNet designed for radar data inversion by Liu et al[26]. In particular, the former is much more computationally efficient than the method proposed in this paper. In addition, we will investigate also refer to the research of Ali and Cha[5], and use the CNN method to realize the long-term monitoring and detection of tunnel lining defects.

Acknowledgments

The research was supported by the National Key R & D Program of China (No. 2018YFC0406904), Joint Program of the National Natural Science Foundation of China (No. U1806226), The key project of National Natural Science

Foundation of China (No. 51739007), Shandong Provincial Natural Science Foundation (No.ZR2018MEE052), and the Transportation Research Project of Department of Transport of Shaanxi Province in 2019 (19-06K). The research was also partially supported by the EU Horizon 2020 Programme under contract 825619 (AI4EU).

[1] J. Richards, Inspection, maintenance and repair of tunnels: international lessons and practice, Tunnelling and Underground Space Technology 13 (4) (1998) 369–375.

[2] I. W. group on maintenance, repair of underground structures, Report on the damaging effects of water on tunnels during their working life, Tunnelling and underground space technology 6 (1) (1991) 11–76.

[3] D. Kolymbas, P. Wagner, Groundwater ingress to tunnels – The exact analytical solution, Tunnelling and Underground Space Technology 22 (1) (2007) 23–27.

[4] M. A. Meguid, H. Dang, The effect of erosion voids on existing tunnel linings, Tunnelling and Underground Space Technology 24 (3) (2009) 278–286.

[5] R. Ali, Y.-J. Cha, Subsurface damage detection of a steel bridge using deep learning and uncooled micro-bolometer, Construction and Building Materials 226 (2019) 376–387.

[6] S. Popovics, J. L. Rose, J. S. Popovics, The behaviour of ultrasonic pulses in concrete, Cement and Concrete Research 20 (2) (1990) 259–270.

[7] Y. Le Sant, M. Marchand, P. Millan, J. Fontaine, An overview of infrared thermography techniques used in large wind tunnels, Aerospace science and technology 6 (5) (2002) 355–366.

[8] A. G. Davis, M. K. Lim, C. G. Petersen, Rapid and economical evaluation of concrete tunnel linings with impulse response and impulse radar non-destructive methods, NDT & E International 38 (3) (2005) 181–186.

[9] P. Holub, T. Dumitrescu, Detection of cavities using electrical parameters and georadar in a water delivery tunnel, Journal of Applied Geophysics 31 (1-4) (1994) 185–195.

[10] M. Kuloglu, C.-C. Chen, Ground penetrating radar for tunnel detection, in: 2010 IEEE International Geoscience and Remote Sensing Symposium, IEEE, 2010, pp. 4314–4317.

[11] F. Zhang, X. Xie, H. Huang, Application of ground penetrating radar in grouting evaluation for shield tunnel construction, Tunnelling and Underground Space Technology 25 (2) (2010) 99–107.

[12] A. M. Alani, F. Tosti, GPR applications in structural detailing of a major tunnel using different frequency antenna systems, Construction and Building Materials 158 (2018) 1111–1122.

[13] S. Jazayeri, S. Kruse, I. Hasan, N. Yazdani, Reinforced concrete mapping using full-waveform inversion of GPR data, Construction and Building Materials 229 (2019) 117102.

[14] F. Zhang, B. Liu, L. Liu, J. Wang, C. Lin, L. Yang, Y. Li, Q. Zhang, W. Yang, Application of ground penetrating radar to detect tunnel lining defects based on improved full waveform inversion and reverse time migration, Near Surface Geophysics 17 (2) (2019) 127–139.

[15] E. Pasolli, F. Melgani, M. Donelli, Automatic analysis of GPR images: A pattern-recognition approach, IEEE Transactions on Geoscience and Remote Sensing 47 (7) (2009) 2206–2217.

[16] X. Xie, P. Li, H. Qin, L. Liu, D. C. Nobes, GPR identification of voids inside concrete based on the support vector machine algorithm, Journal of Geophysics and Engineering 10 (3) (2013) 034002.

[17] Q. Dou, L. Wei, D. R. Magee, A. G. Cohn, Real-time hyperbola recognition and fitting in GPR data, IEEE Transactions on Geoscience and Remote Sensing 55 (1) (2016) 51–62.

[18] X. Zhou, H. Chen, J. Li, An automatic GPR B-scan image interpreting model, IEEE Transactions on Geoscience and Remote Sensing 56 (6) (2018) 3398–3412.

[19] J. Long, E. Shelhamer, T. Darrell, Fully convolutional networks for semantic segmentation, in: Proceedings of the IEEE conference on computer vision and pattern recognition, 2015, pp. 3431–3440.

[20] O. Ronneberger, P. Fischer, T. Brox, U-net: Convolutional networks for biomedical image segmentation, in: International Conference on Medical image computing and computer-assisted intervention, Springer, 2015, pp. 234–241.

[21] V. Badrinarayanan, A. Kendall, R. Cipolla, Segnet: A deep convolutional encoder-decoder architecture for image segmentation, IEEE transactions on pattern analysis and machine intelligence 39 (12) (2017) 2481–2495.

[22] Y. Xu, T. Mo, Q. Feng, P. Zhong, M. Lai, I. Eric, C. Chang, Deep learning of feature representation with multiple instance learning for medical image analysis, in: 2014 IEEE international conference on acoustics, speech and signal processing (ICASSP), IEEE, 2014, pp. 1626–1630.

[23] B. Kayalibay, G. Jensen, P. van der Smagt, CNN-based segmentation of medical imaging data, arXiv preprint arXiv:1701.03056.

[24] S. Li, B. Liu, Y. Ren, Y. Chen, S. Yang, Y. Wang, P. Jiang, Deep-learning inversion of seismic data, IEEE Transactions on Geoscience and Remote Sensing 58 (3) (2020) 2135–2149.

[25] B. Liu, Q. Guo, S. Li, B. Liu, Y. Ren, Y. Pang, L. Liu, P. Jiang, Deep learning inversion of electrical resistivity data, IEEE Transactions on Geoscience and Remote Sensing 58 (8) (2020) 5715–5728.

[26] B. Liu, Y. Ren, H. Liu, H. Xu, Z. Wang, A. G. Cohn, P. Jiang, Gprinvnet: Deep learning-based ground-penetrating radar data inversion for tunnel linings, IEEE Transactions on Geoscience and Remote Sensing 59 (10) (2021) 8305–8325.

[27] B. Liu, S. Yang, Y. Ren, X. Xu, P. Jiang, Y. Chen, Deep-learning seismic full-waveform inversion for realistic structural models, Geophysics 86 (1) (2021) R31–R44.

[28] Y.-J. Cha, W. Choi, O. Büyüköztürk, Deep learning-based crack damage detection using convolutional neural networks, Computer-Aided Civil and Infrastructure Engineering 32 (5) (2017) 361–378.

[29] Y.-J. Cha, W. Choi, G. Suh, S. Mahmoudkhani, O. Büyüköztürk, Autonomous structural visual inspection using region-based deep learning for detecting multiple damage types, Computer-Aided Civil and Infrastructure Engineering 33 (9) (2018) 731–747.

[30] W. Choi, Y.-J. Cha, Sddnet: Real-time crack segmentation, IEEE Transactions on Industrial Electronics 67 (9) (2019) 8016–8025.

[31] X. Miao, J. Wang, Z. Wang, Q. Sui, Y. Gao, P. Jiang, Automatic recognition of highway tunnel defects based on an improved U-net model, IEEE Sensors Journal 19 (23) (2019) 11413–11423.

[32] W. Al-Nuaimy, Y. Huang, M. Nakhkash, M. Fang, V. Nguyen, A. Eriksen, Automatic detection of buried utilities and solid objects with GPR using neural networks and pattern recognition, Journal of applied Geophysics 43 (2-4) (2000) 157–165.

[33] X. Xu, Y. Lei, F. Yang, Railway subgrade defect automatic recognition method based on improved Faster R-CNN, Scientific Programming 2018.

[34] Z. Tong, J. Gao, H. Zhang, Recognition, location, measurement, and 3D reconstruction of concealed cracks using convolutional neural networks, Construction and Building Materials 146 (2017) 775–787.

[35] Z. Tong, J. Gao, D. Yuan, Advances of deep learning applications in ground-penetrating radar: A survey, Construction and Building Materials 258 (2020) 120371.

[36] J. L. Davis, A. P. ANNAN, Ground-penetrating radar for high-resolution mapping of soil and rock stratigraphy 1, Geophysical prospecting 37 (5) (1989) 531–551.

[37] Y. Gao, Y. Jiang, B. Li, Estimation of effect of voids on frequency response of mountain tunnel lining based on microtremor method, Tunnelling and Underground Space Technology 42 (2014) 184–194.

[38] T. Yu, A. Zhu, Y. Chen, Efficient crack detection method for tunnel lining surface cracks based on infrared images, Journal of Computing in Civil Engineering 31 (3) (2016) 04016067.

[39] J. A. Roden, S. D. Gedney, Convolution PML (CPML): An efficient FDTD implementation of the CFS–PML for arbitrary media, Microwave and Optical Technology Letters 27 (5) (2000) 334–339.

[40] L.-C. Chen, G. Papandreou, F. Schroff, H. Adam, Rethinking atrous convolution for semantic image segmentation (2017). `arXiv:1706.05587`.

[41] L.-C. Chen, G. Papandreou, I. Kokkinos, K. Murphy, A. L. Yuille, DeepLab: Semantic Image Segmentation with Deep Convolutional Nets, Atrous Convolution, and Fully Connected CRFs, IEEE Transactions on Pattern Analysis and Machine Intelligence 40 (4) (2018) 834–848.

[42] L.-C. Chen, Y. Zhu, G. Papandreou, F. Schroff, H. Adam, Encoder-decoder with atrous separable convolution for semantic image segmentation, in: Proceedings of the European conference on computer vision (ECCV), 2018, pp. 801–818.

[43] M. Berman, A. Rannen Triki, M. B. Blaschko, The Lovász-Softmax loss: A tractable surrogate for the optimization of the intersection-over-union measure in neural networks, in: Proceedings of the IEEE Conference on Computer Vision and Pattern Recognition, 2018, pp. 4413–4421.

[44] B. Eerapu, Karuna Kumari Ashwath, S. Lal, F. Dell'Acqua, A. N. Dhan, Dense refinement residual network for road extraction from aerial imagery data, IEEE Access 7 (2019) 151764–151782.

[45] G. E. Hinton, N. Srivastava, A. Krizhevsky, I. Sutskever, R. Salakhutdinov, Improving neural networks by preventing co-adaptation of feature detectors, CoRR abs/1207.0580. `arXiv:1207.0580`.

[46] A. Krogh, J. A. Hertz, A simple weight decay can improve generalization, in: Advances in neural information processing systems, 1992, pp. 950–957.

[47] A. Garcia-Garcia, S. Orts-Escolano, S. Oprea, V. Villena-Martinez, J. Garcia-Rodriguez, A review on deep learning techniques applied to semantic segmentation, arXiv preprint arXiv:1704.06857.

[48] D. R. Martin, C. C. Fowlkes, J. Malik, Learning to detect natural image boundaries using local brightness, color, and texture cues, IEEE Transactions on Pattern Analysis & Machine Intelligence (5) (2004) 530–549.

[49] L.-C. Chen, Y. Zhu, G. Papandreou, F. Schroff, H. Adam, Encoder-decoder with atrous separable convolution for semantic image segmentation, in: The European Conference on Computer Vision (ECCV), 2018.

[50] C. Sivaji, O. Nishizawa, G. Kitagawa, Y. Fukushima, A physical-model study of the statistics of seismic waveform fluctuations in random heterogeneous media, Geophysical Journal International 148 (3) (2002) 575–595.

[51] B. Liu, Y. Pang, D. Mao, J. Wang, Z. Liu, N. Wang, S. Liu, X. Zhang, A rapid four-dimensional resistivity data inversion method using temporal segmentation, Geophysical Journal International 221 (1) (2020) 586–602.

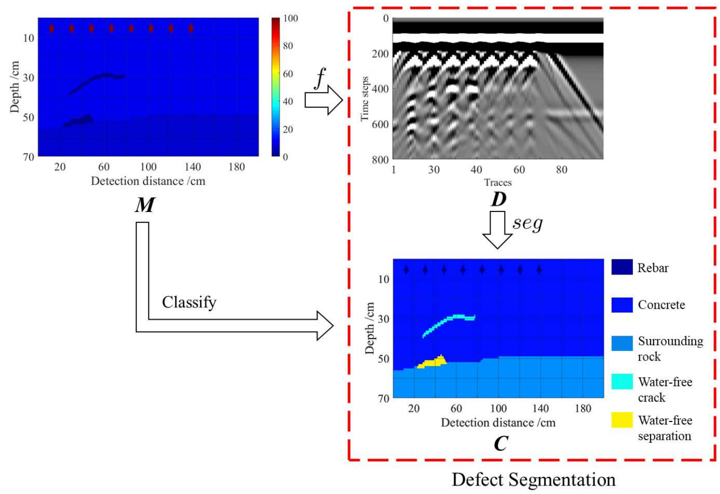

Figure 1: Defect segmentation method. The numerical model M was designed, and the GPR data D was obtained by modeling. Then, using the model M, the defect segmentation model C was obtained and used as a label for training the CNN. Our defect segmentation method trains the CNN to get the mapping relationship seg and complete the calculation of C from D.

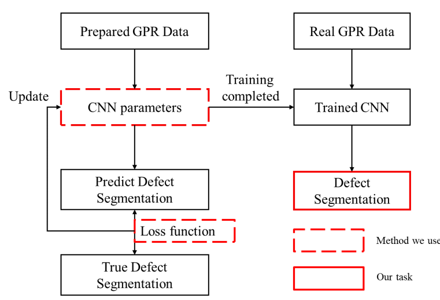

Figure 2: Workflow of the CNN based segmentation method. Prepared GPR data is input into the CNN, and the predicted result, based on current CNN parameters, is obtained. The difference between the prediction result and the actual model is calculated by the loss function, and the CNN parameters are updated by the gradient. The CNN is trained after multiple iterations. After inputting the GPR data, the CNN parameters can be used to obtain the fault segmentation directly.

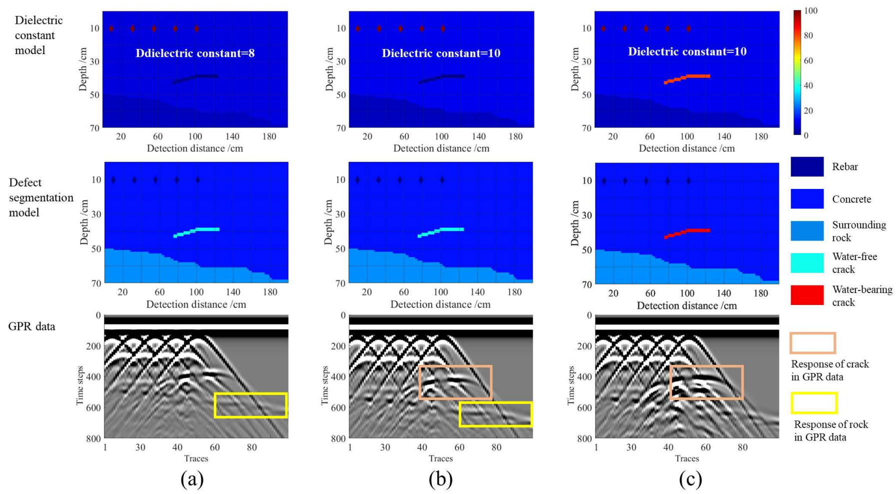

Figure 3: Models with the same structure and different dielectric constants, as well as the GPR data that goes with them. Both (a) and (b) represent the dielectric constant model of a water-free crack, corresponding defect segmentation model and GPR data; the difference between (a) and (b) lies in the fact that the dielectric constant values of their surrounding rocks are different, which leads to differences in GPR data; (c) represents the dielectric constant model of a water-bearing crack, corresponding defect segmentation model, and GPR data.

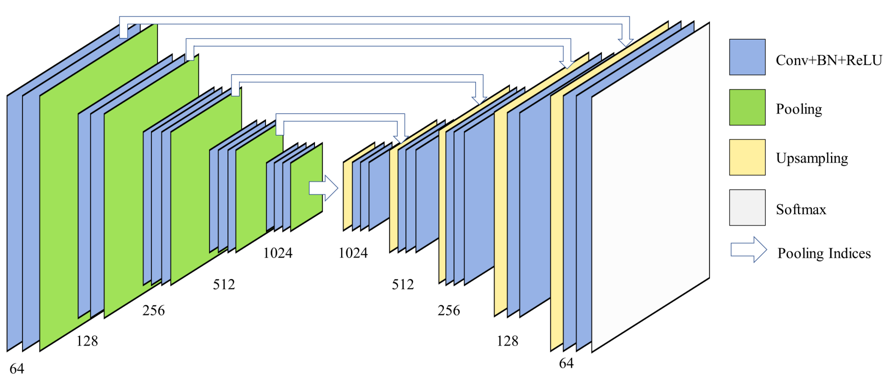

Figure 4: Segnet structure.

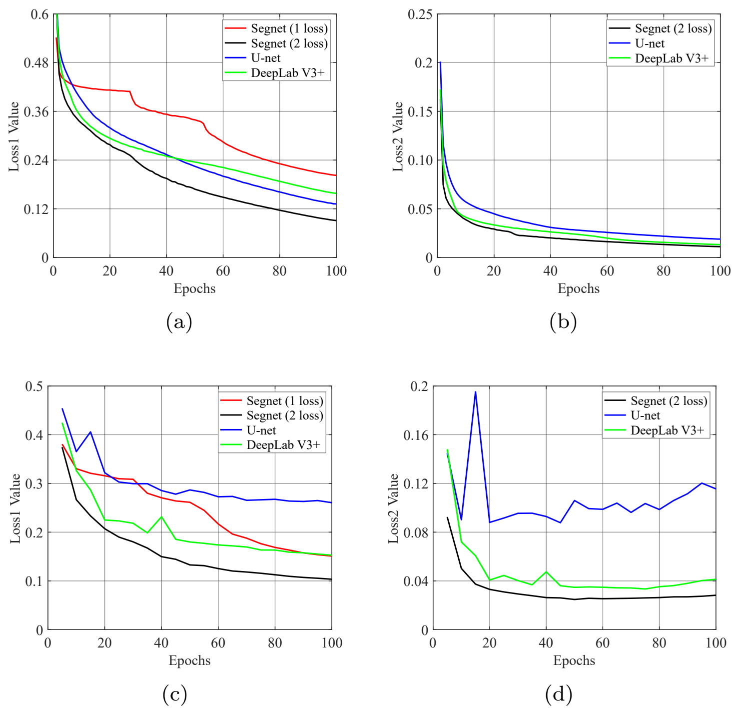

Figure 5: Loss curves of the three CNN methods. (a) and (b) are the curves of the cross-entropy loss function (Loss 1) and the Lovász softmax loss function (Loss 2) on the training set with epoch, respectively. (c) and (d) are the curves of the cross-entropy loss function (Loss 1) and the Lovász softmax loss function (Loss 2) on the validation set with epoch, respectively. In these graphs the red, black, blue, and green lines represent Segnet (1 loss), Segnet(2 loss), U-net, and DeepLab V3+ respectively.

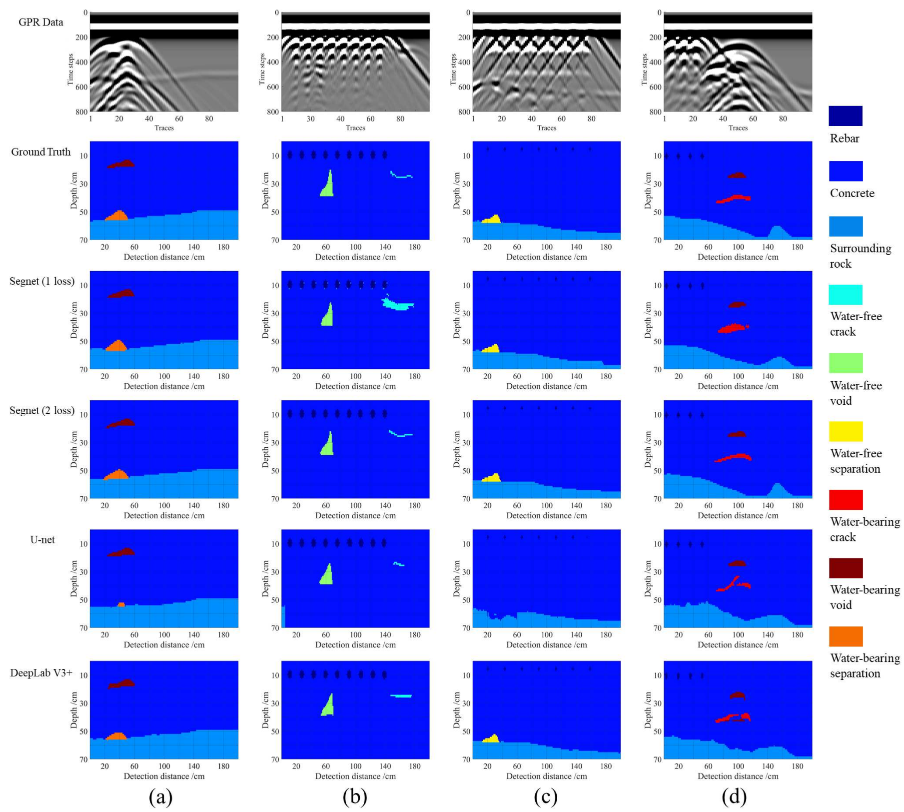

Figure 6: Prediction results of three methods on test data. There are four sets of data, ground truth, and prediction results of Segnet(1 loss), Segnet(2 loss), U-net, and DeepLab V3+.

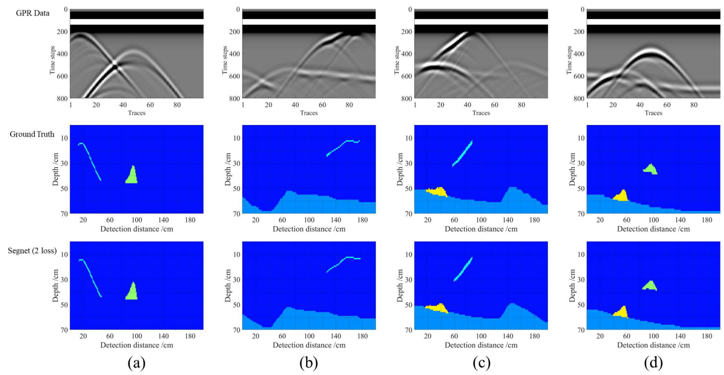

Figure 7: Water-free defects in the tunnel lining without rebar model prediction results. (a) represents the water-free crack and void model without surrounding rock. (b) represents the water-free crack model. (c) represents the water-free crack and separation model. (d) represents the water-free void and separation model. Each color represents the same material as in Fig. 6.

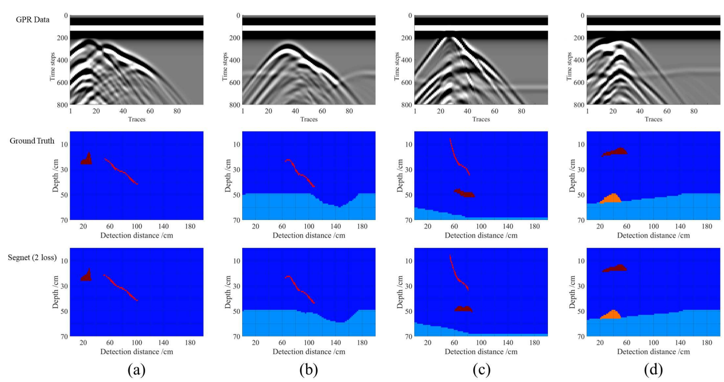

Figure 8: Prediction results on a non reinforced model with water-bearing defects in tunnel lining. (a) represents the water-bearing crack and void model without surrounding rock. (b) represents the water-bearing crack model. (c) represents the water-bearing crack and separation model. (d) represents the water-bearing void and separation model. Each color represents the same material as in Fig. 6.

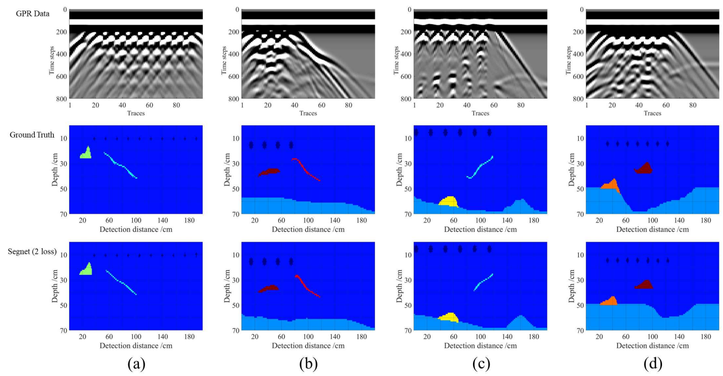

Figure 9: Water-bearing defects in the tunnel lining without rebar model prediction results. (a) represents the water-free crack and void model with rebars. (b) represents the water-bearing crack and void model with rebars. (c) represents the water-free crack and separation model with rebars. (d) represents the water-bearing void and separation model with rebars. Each color represents the same material as in Fig. 6.

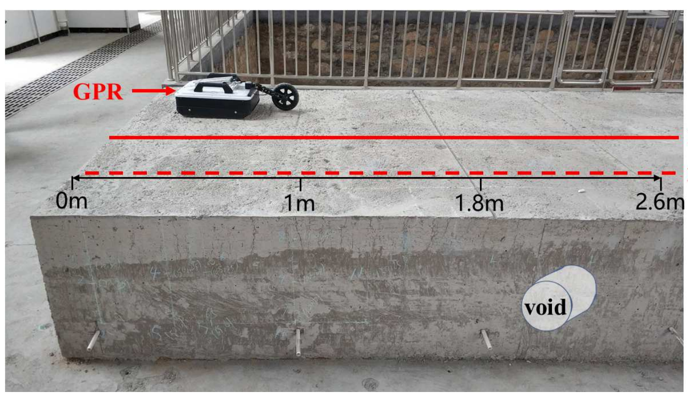

Figure 10: The model we built and GPR for detection.

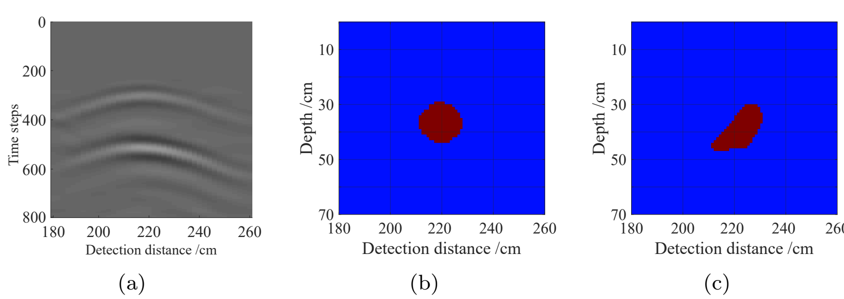

Figure 11: Results of the real GPR data. (a), (b), and (c) represent measured GPR data, corresponding model, and the model prediction respectively.